Available online at www.sciencedirect.com

ScienceDirect

IFAC Papers Online CONFERENCE PAPER ARCHIVE

IFAC-PapersOnLine 48-15 (2015) 159–166

On Beneficial Mode Switch Decisions based on Short-term Engine Load Prediction ⋆

Sandro P. Nüesch * **Jeff Sterniak** ** **Li Jiang** **
Anna G. Stefanopoulou *

* *Dept. of Mechanical Engineering, University of Michigan, Ann Arbor, MI 48109 USA (e-mail: snuesch@umich.edu).*
** *Robert Bosch LLC, Farmington Hills, MI 48331 USA.*

Abstract: Multimode combustion in automotive engines have the potential to increase fuel efficiency by choosing the best combustion mode at each operating condition. When switches among the combustion modes are neither instantaneous nor lossless, a mode switch can only be beneficial if the associated residence time in the target mode is long enough to compensate for the fuel penalty of the switch. An accurate engine load prediction over a short-term horizon is thus necessary for deciding on a beneficial mode switch. This paper addresses this. In the application of spark ignited (SI) and homogeneous charge compression ignition (HCCI) combustion modes, prior work quantified fuel efficiency benefits and mode switch penalties. In this paper, it is estimated that, to result in a fuel economy benefit, the residence time in HCCI mode is required to be longer than 1.2 s. If it is possible to accurately predict engine load over such a time horizon, an optimal mode switch decision could be made. To this end, five receding horizon prediction methods, based on artificial neural networks and polynomial extrapolation, are tested with vehicle measurement data and compared in terms of their accuracy in predicting engine load as well as HCCI entry and exit events. It is shown that although the prediction accuracy is very low for visitations of the HCCI regime around 1.2 s, all the methods are able to determine if an immediate entry of exit will occur, and if a HCCI visitation is going to be very short. This finding is applied in a basic mode switch decision structure.

Keywords: Advanced combustion, Engine control, Supervisory control, Combustion mode switches, Prediction methods, Artificial neural networks

1. INTRODUCTION

Advanced combustion modes such as homogeneous charge compression ignition (HCCI) have significant benefits in fuel efficiency and engine-out NOx emissions, as shown by Zhao et al. (2003). However, they have a limited operating range and are not able to fulfill all the drivers demands, see Thring (1989). For that reason they are combined with spark ignition (SI) combustion in a multimode combustion engine, which switches the mode based on operating condition, as suggested by Kulzer et al. (2007). SI and HCCI combustion are radically different, and the mode switch from one to the other is a difficult control task, shown by Gorzelic et al. (2014) and Zhang and Zhu (2014). Those mode switches require a certain duration and, as shown in Matsuda et al. (2008), incur a fuel penalty. Based on Nüesch et al. (2014) it can be seen that during a conventional drive cycle some residence times in the HCCI mode are very short and due to the switching penalty in fact harmful for overall fuel economy. A supervisory control strategy is required to decide when a mode switch should be performed. Such a strategy could be based on the prediction of future operating conditions, thereby making an optimum decision in terms of fuel economy.

In Sun et al. (2014) several methods to predict vehicle speed are compared in the context of hybrid electric vehicles (HEV). By applying model predictive control the predictions are used to determine the optimal power split while obeying constraints on battery state-of-charge. Even though the problem of optimal HEV power management shows similarities to the one of optimal combustion mode switching, there are significant differences. First, the impact of non-optimal decisions are different. In the HEV problem a prediction error might lead to a temporarily wrong power split. However, the supervisory controller will

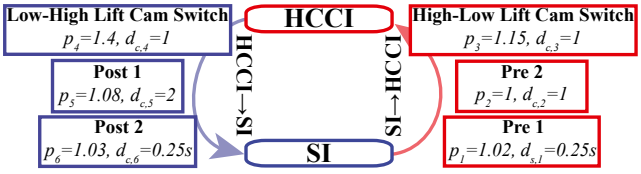

Fig. 1. Reduced representation of the combustion mode switch model from Nüesch et al. (2015). Shown are the values for fuel penalties p_i, and durations $d_{s,i}$ and $d_{c,i}$ in seconds and engine cycles, respectively.

⋆ This material is based upon work supported by the Department of Energy [National Energy Technology Laboratory] under Award Number(s) DE-EE0003533. This work is performed as a part of the ACCESS project consortium (Robert Bosch LLC, AVL Inc., Emitec Inc., Stanford University, University of Michigan) under the direction of PI Hakan Yilmaz and Co-PI Oliver Miersch-Wiemers, Robert Bosch LLC.

10.1016/j.ifacol.2015.10.023

generally get the opportunity to compensate for the mistake later, thereby limiting the impact of a wrong decision. In case of the multimode combustion problem this is not possible. If a mode switch decision is wrong, the associated opportunity for fuel economy benefits has passed. Second, in the power split case a trend-wise correct prediction is enough to achieve satisfactory controller performance. However, in the case of mode switches, precise prediction of the direction and magnitude of the operating conditions is necessary to achieve the optimal switching decision. In Nüesch et al. (2015) it is shown that the majority of mode switches are due to the dynamics in engine load rather than engine speed. For that reason in this paper it is focused on methods of predicting engine load, and perfect knowledge of future engine speed is assumed. Even if elevation changes are taken into account, it can be assumed that the fast dynamics in engine load are mainly caused by the driver. It can be expected that a model might not be able to perfectly mimic a human driver and compared to the more erratic human behavior, a model might be more predictable. Therefore, the assessment in this paper is done from actual measurements from a drive cycle with a human driver rather than a driver model.

In Sect. 2 the engine and vehicle data is described, and in Sect. 3 the required minimum duration of a stay in HCCI mode is estimated. Sect. 4 introduces the different prediction methods, which are assessed in Sect. 5, followed by a brief discussion in Sect. 6.

2. DATA

2.1 Engine Data

In this paper a 2.0 L I4 multimode combustion engine with a stock turbocharger is used. Compared to the production version (GM Ecotec LNF) the engine includes increased compression ratio, two-step cam profile switching, electric cam phasing for recompression, and stronger reciprocating components. This enables naturally aspirated (NA) HCCI, as well as traditional SI mode. Note that advanced combustion strategies, such as multi injection and multi ignition (MIMI) or boosted HCCI can expand the HCCI operating regime beyond the NA basic HCCI region used in this paper. A combustion mode switch model, based on a finite state machine, was introduced in Nüesch et al. (2014) and parameterized with experiments in Nüesch et al. (2015). A simplified version of this model, reduced to the six significant transition states i, is depicted in Fig. 1. The associated parameters are fuel penalties p_i as well as durations $d_{s,i}$ in seconds and $d_{c,i}$ in engine cycles. Engine speed n in RPM relates the two durations with

$$d_{s,i} = d_{c,i} \cdot \frac{2 \cdot 60}{n}. \tag{1}$$

2.2 Drive Cycle Data

Chassis dynamometer measurements for FTP75, HWFET, and US06 drive cycles were used, acquired with a stock Cadillac CTS 2009. The measured velocity data is denoted $\bar{v}$, the measured engine torque and speed data are $\bar{T}$ and $\bar{n}$, respectively. The selected gear is $\bar{g}$. Note that the drive cycle data does not originate from the multimode engine but from the larger 3.6 L V6 stock engine. However, it

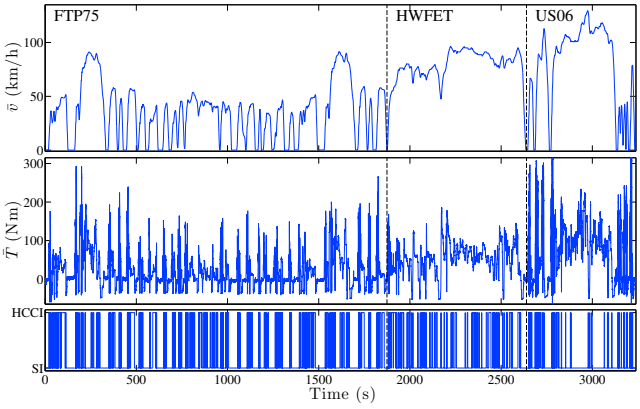

Fig. 2. Vehicle measurements for FTP75, HWFET, and US06 drive cycles. Top: Velocity $\bar{v}$. Center: Engine torque $\bar{T}$. Bottom: Combustion Regime.

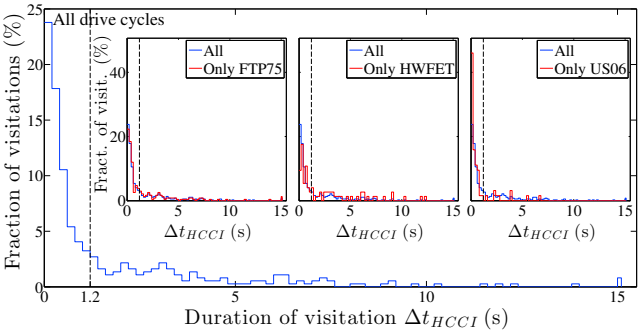

Fig. 3. Distribution of visitation durations in the HCCI regime. Large: Combined. Insets: Individual drive cycles.

is assumed that, given vehicle and drive cycle, the load requirement from the driver to the downsized engine is similar to the one seen by the stock one. In any case the applied prediction methods need to be accurate under varying driver and engine behavior.

Velocity and engine load for all three drive cycles are shown in Fig. 2. In addition every stay in the HCCI operating regime is highlighted. It should be noted that the cold-start period at the beginning of the FTP75 has been neglected in this study, since it is irrelevant to the problem of load prediction.

The distribution of durations of visitations in the HCCI operating regime is shown in Fig. 3. As can be seen, the distributions strongly depend on the applied drive cycle. The aggressive US06 drive cycle exhibits a significantly larger fraction of short visitations than both the FTP75 and the HWFET cycle.

3. REQUIRED MINIMUM DURATION IN HCCI

Each switch to HCCI and back exhibits a fuel penalty. Therefore the residence time in the HCCI mode Δt_{HCCI} needs to be long enough to result in a net benefit in fuel economy. This duration is denoted required minimum duration of a visitation $\Delta t_{HCCI,min}$.

By using the durations $d_{s,i}$, the total mode switch duration $d_{s,tot}(n)$ as a function of engine speed is calculated, which includes both, the SI-HCCI and the HCCI-SI direction:

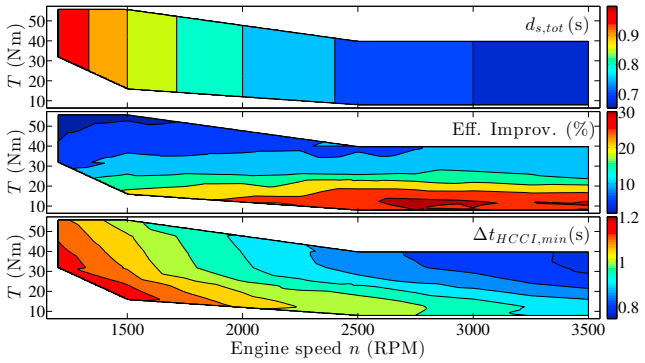

Fig. 4. HCCI operating regime. Top: Total mode switch duration $d_{s,tot}$ based on the combustion mode switch model. Center: Fuel efficiency improvement of HCCI compared to SI combustion based on measurements. Bottom: Minimum time spent in HCCI to lead to fuel economy benefit $\Delta t_{HCCI,min}$.

$$d_{s,tot}(n) = \sum_{i=1}^{6} d_{s,i}. \tag{2}$$

It must be noted that, since as of now only experimental mode switch data at one operating condition is available, the parameters are constant in terms of n and T, which leads to the linearly changing $d_{s,tot}$ in Fig. 4-top. Based on the fuel efficiency map the fuel flows $\dot{m}_{f,SI}(n,T)$, $\dot{m}_{f,HCCI}(n,T)$ are calculated. The relative improvement of the fuel efficiency in HCCI compared to SI is shown in Fig. 4-center. The minimum duration in HCCI mode to lead to a net fuel economy benefit $\Delta t_{HCCI,min}(n,T)$ follows as:

$$m_{f,Pen}(n,T) = \left(\sum_{i=1}^{6} p_i \cdot \Delta t_i\right) \cdot \dot{m}_{f,SI} \tag{3}$$

$$\Delta t_{HCCI,min}(n,T) = \frac{m_{f,Pen}}{\dot{m}_{f,HCCI}} \tag{4}$$

In Fig. 4-bottom the map of $\Delta t_{HCCI,min}(n,T)$ is shown. As can be seen at higher engine speeds a visitation of the HCCI regime needs to be be at least around 0.8 s to be beneficial. With decreasing speed this value increases up to 1.2 s. If a stay in HCCI is predicted to be longer than 1.2 s it is ensured that the stay will be beneficial. Vice versa if the stay in HCCI is predicted to be shorter than 0.8 s. Note that these numbers do not include other fuel penalties, e.g. due to the depletion of the catalyst's oxygen storage. Such additional penalties could increase $\Delta t_{HCCI,min}$ significantly.

As can be seen in Fig. 3, a large fraction of stays is either longer than 1.2 s or much shorter. Here prediction can resolve the trade-off between switching to HCCI as early as possible and avoiding very short residences in HCCI mode. For the cases $0.8\,\text{s} < \Delta t_{HCCI} < 1.2\,\text{s}$ the fuel consumption needs to be predicted to make an optimal decision. It has to be noted that this analysis assumes constant load and speed during the entire visitation of HCCI, which does not occur in reality. Nevertheless it gives a good estimate for the prediction horizon needed to make an optimal mode switch decision.

4. ENGINE LOAD HORIZON PREDICTORS

Five receding horizon methods for torque prediction are compared. Two of them apply Artificial Neural Networks (ANN) and are labeled with A. Neural networks have been used successfully to forecast timeseries of nonlinear behavior. The prediction of an ANN depends on its tuning. However, a set of ANNs based different tuning parameters all resulted in comparable performance with the selected ones being the best. The other three methods use linear least squares to compute linear and quadratic polynomial fits P_1 and P_2, respectively. In further distinction, the methods labeled with V are based on the velocity history to predict future velocities and, by using a vehicle model, to compute the future engine torque trajectory. Conversely, the methods denoted T are based on using the engine torque history directly to predict future torque. All the methods are described in detail below.

Based on the result for $\Delta t_{HCCI,min}$ a prediction horizon length H is chosen for all the methods such that

$$\tau_1 \cdot H = 2\,\text{s} \tag{5}$$

with sampling time $\tau_1 = 0.01\,\text{s}$. Velocity and engine torque at time step k are denoted

$$v_k = v(k\tau)\ ;\ T_k = T(k\tau). \tag{6}$$

At each time step k the receding horizon of engine torque $\mathbf{T}_k$ is calculated

$$\mathbf{T}_k = \left(\widehat{T}^k_{k+1}, \widehat{T}^k_{k+2}, ..., \widehat{T}^k_{k+H}\right)^{\mathrm{T}} \tag{7}$$

with predicted torque $\widehat{T}^k_{k+j}$ at j time steps after current time k.

4.1 ANN Torque Predictor (A/T)

The ANN to predict future torque is denoted $f_{A/T}$, using historical torque data $\bar{T}$ as input to compute torque predictions $\hat{T}$. At each time step k the receding horizon of engine torque $\mathbf{T}^{A/T}_k$ is calculated:

$$\mathbf{T}^{A/T}_k = f_{A/T}(\bar{T}_{k-h}, ..., \bar{T}_{k-2}, \bar{T}_{k-1}, \bar{T}_k) \tag{8}$$

The history for the torque predictor was chosen $h \cdot \tau_1 = 1\,\text{s}$. The ANN $f_{A/T}$ was trained based on the measured torque data shown in Fig. 2. The network consist of 15 hidden layers. 70% of the dataset, sampled with 0.1 s, was used for training, based on the Levenberg-Marquardt method.

4.2 Linear Torque Predictor (P_1/T)

The linear least squares methods is used to create a linear fit of engine torque with matrices A_1 and W and based on the history $h \cdot \tau_1 = 0.5\,\text{s}$ with weighting factor $a = 10$:

$$\mathbf{T}^{hist}_k = \left(\,\bar{T}_{k-h}, ..., \bar{T}_{k-2}, \bar{T}_{k-1}, \bar{T}_k\,\right)^{\mathrm{T}} \tag{9}$$

$$\mathbf{A}_1 = \left(\,-h\cdot\tau_1, -(h-1)\tau_1, \ldots, -\tau_1, 0\,\right)^{\mathrm{T}} \tag{10}$$

$$\mathbf{W} = \begin{pmatrix} e^{-a\cdot h\cdot\tau_1} & 0 & 0 & 0 \\ 0 & e^{-a\cdot(h-1)\cdot\tau_1} & 0 & 0 \\ & & \ddots & 0 \\ 0 & 0 & 0 & 1 \end{pmatrix}. \tag{11}$$

The polynomial is constrained to the initial engine torque T_k. The slope of the torque trajectory $x_k^{P_1/T}$ at each time step follows by solving:

$$(\mathbf{A}_1^{\mathrm{T}}\mathbf{W}\mathbf{A}_1)x_k^{P_1/T} = \mathbf{A}_1^{\mathrm{T}}\mathbf{W}(\mathbf{T}_k^{hist} - \bar{T}_k). \quad (12)$$

Finally the receding torque horizon follows as

$$\mathbf{T}_k^{P_1/T} = \bar{T}_k + x_k^{P_1/T} \cdot (0, \tau_1, \ldots, H \cdot \tau_1)^{\mathrm{T}}. \quad (13)$$

4.3 Quadratic Torque Predictor (P_2/T)

The quadratic torque predictor is based on the same principle as the linear one and uses a history $h \cdot \tau_1 = 0.5\,\mathrm{s}$ with weighting factor $a = 10$. However, in addition to the slope $x_k^{P_2/T,1}$ the curvature $x_k^{P_2/T,2}$ is computed:

$$\mathbf{A}_2 = \begin{pmatrix} -h \cdot \tau_1, -(h-1)\tau_1, \ldots, -\tau_1, 0 \\ (h \cdot \tau_1)^2, ((h-1) \cdot \tau_1)^2, \ldots, \tau_1^2, 0 \end{pmatrix}^{\mathrm{T}} \quad (14)$$

$$\mathbf{A}_2^{\mathrm{T}}\mathbf{W}\mathbf{A}_2 \begin{pmatrix} x_k^{P_2/T,1} \\ x_k^{P_2/T,2} \end{pmatrix} = \mathbf{A}_2^{\mathrm{T}}\mathbf{W}(\mathbf{T}_k^{hist} - \bar{T}_k) \quad (15)$$

$$\mathbf{T}_k^{P_2/T} = \bar{T}_k + x_k^{P_2/T,1} \cdot (0, \tau_1, \ldots, H \cdot \tau_1)^{\mathrm{T}} \ldots \quad (16)$$

$$+ x_k^{P_2/T,2} \cdot \left(0, \tau_1^2, \ldots, (H \cdot \tau_1)^2\right)^{\mathrm{T}}. \quad (17)$$

4.4 ANN Velocity Predictor (A/V)

The following predictor is based on the ANN $f_{A/V}$, trained with the measured velocity data shown in Fig. 2. Training conditions of the ANN are the same as above for $f_{A/T}$. The velocity history is chosen to be $h \cdot \tau_1 = 3\,\mathrm{s}$. At each time step k, based on current velocity $\bar{v}_k$ and h historical values, the receding velocity horizon $\mathbf{v}_k^{A/V}$ is calculated:

$$\mathbf{v}_k^{A/V} = f_{A/V}(\bar{v}_{k-h}, ..., \bar{v}_{k-2}, \bar{v}_{k-1}, \bar{v}_k) \quad (18)$$

$$= \left(\widehat{v}_{k+1}^k, \widehat{v}_{k+2}^k, ..., \widehat{v}_{k+H}^k\right)^{\mathrm{T}}. \quad (19)$$

The quasi-static vehicle model f_v is used to compute engine torque as a function of velocity and gear:

$$\hat{T}_k = f_v(\bar{v}_k, \bar{g}_k). \quad (20)$$

The model f_v relies on differentiation of the velocity using finite differences to compute acceleration and therefore propulsion torque. It is compared to measurements in Fig. 5. As can be seen the general behavior of T is reproduced well. However, the model filters some of the fast torque dynamics, one reason being a higher sampling frequency for torque compared to velocity during data acquisition.

The gear over the receding horizon is assumed to be constant at the recorded value $\bar{g}_k$. The difference at k between computed and actual torque $\widetilde{T}_k$, due to modeling errors and uncertainties, can be calculated

$$\widetilde{T}_k = \bar{T}_k - \widehat{T}_k \quad (21)$$

and therefore the entire prediction can be shifted, finally leading to

$$\mathbf{T}_k^{A/V} = f_v(\mathbf{v}_k^{A/V}, \bar{g}_k) + \widetilde{T}_k. \quad (22)$$

4.5 Quadratic Velocity Predictor (P_2/V)

The quadratic velocity predictor is fitted over a history $h \cdot \tau_s = 1\,\mathrm{s}$ and the weights are exponentially decaying with $a = 5$.

$$\mathbf{v}_k^{hist} = (\,\bar{v}_{k-h}, ..., \bar{v}_{k-2}, \bar{v}_{k-1}, \bar{v}_k\,)^{\mathrm{T}} \quad (23)$$

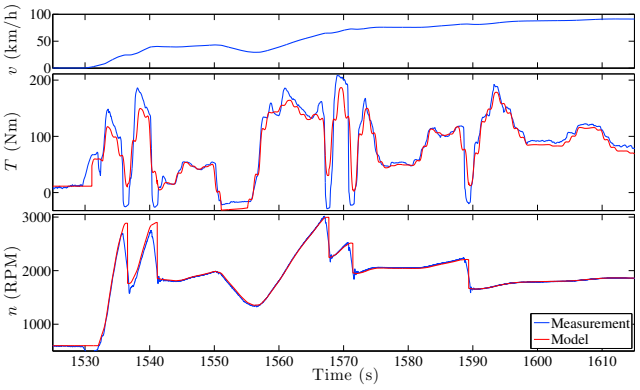

Fig. 5. Vehicle model results (red) compared with chassis dynamometer measurements (blue).

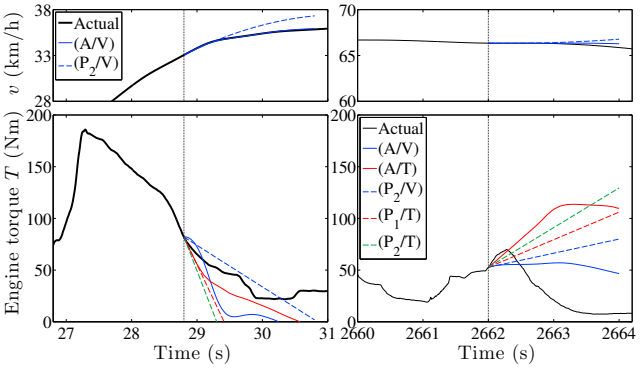

Fig. 6. Velocity and torque prediction result of the five predictors at two example situations.

$$\mathbf{A}_2^{\mathrm{T}}\mathbf{W}\mathbf{A}_2 \begin{pmatrix} x_k^{P_2/V,1} \\ x_k^{P_2/V,2} \end{pmatrix} = \mathbf{A}_2^{\mathrm{T}}\mathbf{W}(\mathbf{v}_k^{hist} - \bar{v}_k) \quad (24)$$

$$\mathbf{v}_k^{P_2/V} = \bar{v}_k + x_k^{P_2/V,1} \cdot (0, \tau_s, \ldots, H \cdot \tau_s)^{\mathrm{T}} \ldots \quad (25)$$

$$+ x_k^{P_2/V,2} \cdot \left(0, \tau_s^2, \ldots, (H \cdot \tau_s)^2\right)^{\mathrm{T}} \quad (26)$$

$$\mathbf{T}_k^{P_2/V} = f_v(\mathbf{v}_k^{P_2/V}, \bar{g}_k) + \widetilde{T}_k. \quad (27)$$

4.6 Examples

Two examples of receding horizons for all predictions methods are shown in Fig. 6. On the left, during an acceleration, all the load predictions are qualitatively correct. Note that (A/V) predicts the velocity profile perfectly and nevertheless results in a relatively large discrepancy in the torque trajectory. On the right, during a coasting phase, none of the methods are able to predict the sudden decrease in load.

Examples of receding torque horizons over a larger time frame are shown in Fig. 7. Generally, the two velocity predictors (A/V) and (P_2/V) (top) forecast the load to remain relatively close to the real value. The predictor (A/T) (left center) shows larger discrepancies with increasing prediction time. The predictions (P_1/T), (P_2/T) (center and bottom right) sometimes show very large slopes leading to extremely high torque predictions towards the end of the horizon. It can be reasoned that the velocity based predictors are able to forecast the general trend in load relatively well. However, the application of the quasi-static

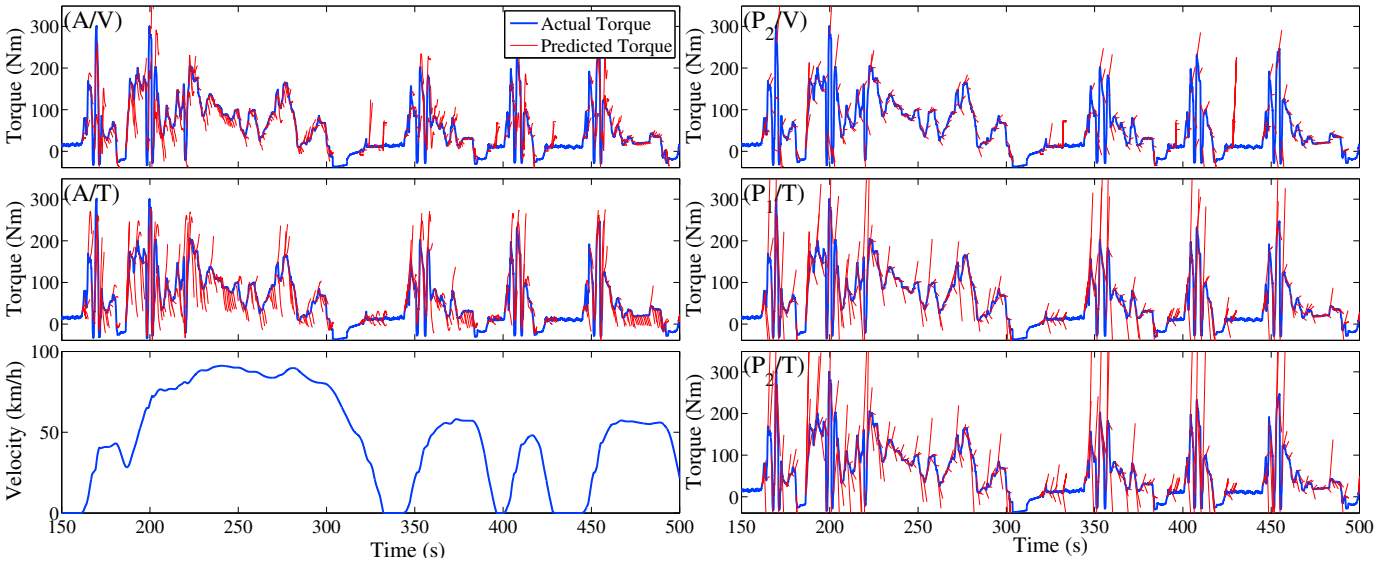

Fig. 7. Torque prediction result of the five predictors for part of the FTP75. The actual torque in shown in blue. The predicted torque is shown in red across the prediction horizon of 2 s at each second. The associated velocity profile is shown in the bottom left plot.

vehicle model as well as the velocity differentiation leads to large uncertainties in the fast torque dynamics. Even a torque forecast based on perfect vehicle speed prediction shows relatively large deviations from the real trajectory. On the other hand, the torque predictors are more suited to forecast the fast torque dynamics. Towards the end of the prediction horizon, however, they often show large deviations from the actual trajectory.

5. COMPARISON OF PREDICTION METHODS

In the following section the five predictors are compared in more detail, first in terms of their general accuracy over the entire load range, then focused on the HCCI load regime and their predictions of entry and exit times.

5.1 General Performance

To quantify the accuracy of the different prediction methods, at each time step k the error E_j^k between the load prediction $\mathbf{T}_k$ and the actual value $\mathbf{T}_k^{Real}$ is calculated, based on the infinity norm of the deviation:

$$\mathbf{T}_k^{Real} = \left(\bar{T}_{k+1}, \bar{T}_{k+2}, ..., \bar{T}_{k+H}\right)^{\mathrm{T}} \tag{28}$$

$$e_j^k = |\bar{T}_{k+j} - \hat{T}_{k+j}^k| \text{ with } j = 1, 2, \ldots, H \tag{29}$$

$$E_j^k = \max\left(e_1^k, \ldots, e_j^k\right). \tag{30}$$

The entire dataset, shown in Fig. 2, was sampled at $\tau_2 = 0.5\,\mathrm{s}$ and a prediction performed for each time step k at which the velocity is nonzero and the load is positive. Note that the time step for the predictions themselves is still τ_1. The distribution of the prediction errors E_j^k for all k was calculated and is shown in Fig. 8 as a function of the receding horizon $j \cdot \tau_1$. The contour lines, representing 3 Nm, 6 Nm, and 9 Nm, are plotted in Fig. 9 to directly compare the five prediction methods. In addition to the five methods the performance of a naive predictor, which simply assumes constant load over the prediction horizon, is shown as well. At the beginning of

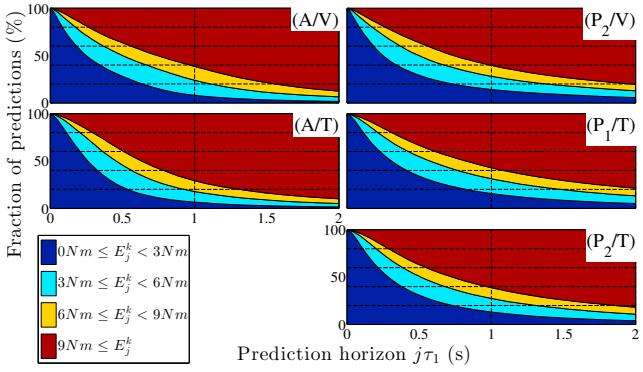

Fig. 8. Distribution of the prediction error E_j^k over the horizon. The plots show the fraction of predictions with $E_j^k < 3\,\mathrm{Nm}$, $E_j^k < 6\,\mathrm{Nm}$, and $E_j^k < 9\,\mathrm{Nm}$.

the prediction most methods are more accurate than the naive predictor. However, the accuracy of all the predictors drops rapidly with increasing j and are outperformed by the naive predictor. Beyond $j\tau_1 > 0.5\,\mathrm{s}$ less than 40% of predictions show $E_j^k < 3\,\mathrm{Nm}$. At the end of the prediction horizon at $j\tau_1 = 2\,\mathrm{s}$ the number of accurate predictions is below 5%. The fraction of predictions, that are still somewhat accurate with $E_j^k < 9\,\mathrm{Nm}$, is higher and at best 20%. All the methods show comparable and relatively poor performance, with (A/T) resulting in the lowest accuracy.

One question is, how the different prediction methods compare for different driving styles and cycles. The analysis from above was conducted for the three drive cycle individually and is shown in Fig. 10. The torque response during the HWFET seems overall to be easier to predict versus one during the US06 cycle. This includes the naive predictor, which simply assumes constant load. Those differences might be due to the characteristics of the drive cycles themselves and their number of fast accelerations, gearshifts, driver behavior, and engine response etc. For

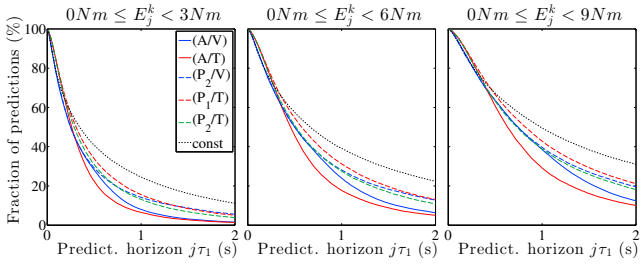

Fig. 9. Distribution of the prediction error over the horizon. The plots show the fraction of predictions with $E_j^k < 3\,\mathrm{Nm}$ (Left), $E_j^k < 6\,\mathrm{Nm}$ (Center), and $E_j^k < 9\,\mathrm{Nm}$ (Right).

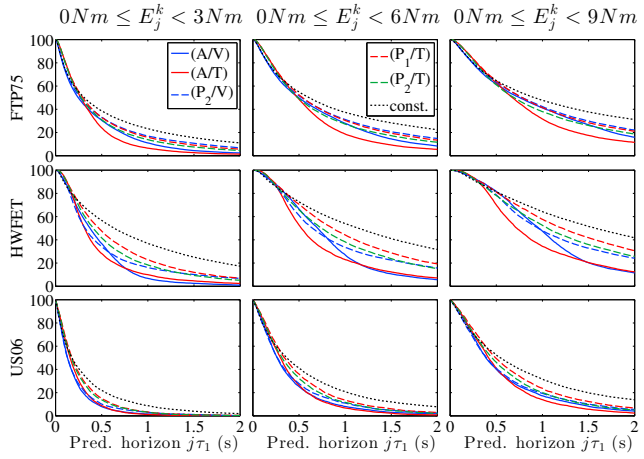

Fig. 10. Distribution of the prediction error over the horizon for the three individual drive cycles. The plots show the fraction of predictions with $E_j^k < 3\,\mathrm{Nm}$ (Left), $E_j^k < 6\,\mathrm{Nm}$ (Center), and $E_j^k < 9\,\mathrm{Nm}$ (Right).

example, it is reasonable to assume that a linear fit works well for slow dynamics but poorly for fast ones. In addition, other method-related aspects may play a role. For example the weighting factors of the polynomial fits, the applied training data for the ANNs or the accuracy of the measurements will have an influence. However, based on the variety of methods and drive cycles tested here, we believe the presented trends in terms of short-term load prediction are representative.

5.2 HCCI Performance

The load predictions from above are tested specifically towards their application in SI/HCCI mode switches. They are used to give an estimate of the next entry and exit times in the HCCI operating regime and the associated duration of a stay in the regime. At each time step k, $\mathbf{T}_k$ is used to find the next crossings of either the maximum or the minimum HCCI load boundary. As mentioned above, perfect knowledge of engine speed n is assumed. If at k the engine operates outside the HCCI regime, the duration until the next crossing of the HCCI limits is denoted $t_{Entry,Pred}$. Similarly, the predicted duration until the HCCI regime is left again is denoted $t_{Exit,Pred}$. The annotations are explained in Fig. 11. The subscript *Real* is used for the associated values derived from the actual torque trajectory.

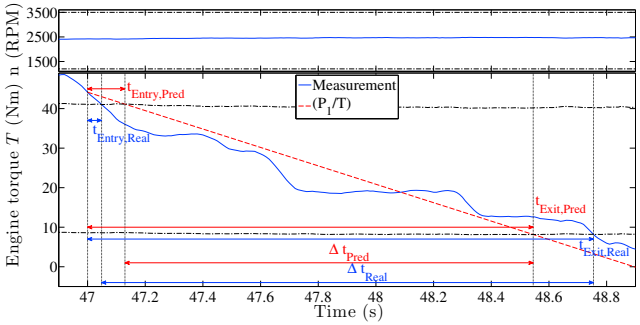

Fig. 11. Annotation for HCCI entry and exit times at example engine speed and load trajectories.

The prediction based entry and exit durations are compared to the actual values in Fig. 12. The durations are separated into different bins from 0 s to 2 s, the end of the horizon. If no crossing is detected within the horizon, the bin is called *No Entry* or *No Exit*. Note that the probabilities for the exit assumes that the prediction is made within the HCCI regime. For a given prediction the probability is calculated at which the prediction lies in the same bin as an actual duration. In case of a perfect prediction the entries on the diagonal would be 100%. The larger the deviation from the diagonal the worse the overall prediction quality. As can be seen in Fig. 12 all the methods show high accuracies between 60-70% in predicting an entry or exit within the next 0.2 s. In addition, the accuracies of no entry and exit predictions are relatively high as well with 77-81% and 50-67%, respectively. However, prediction in-between those two cases show very low accuracy and are throughout too pessimistic.

The duration of the next visitation in HCCI Δt is calculated if at time step k the engine either operates in the HCCI regime or or an entry is predicted to occur shortly:

$$\Delta t = \begin{cases} t_{Exit} - t_{Entry} & t_{Entry} \leq 0.5\,\mathrm{s} \\ t_{Exit} & \text{in HCCI} \\ \text{No calculation} \end{cases} \tag{31}$$

The probabilities for a given predicted HCCI visitation duration Δt_{Pred} are shown in the bottom third of Fig. 12. Note that the shown probabilities assume that an entry within the next 0.5 s is correctly predicted. It can be seen that short visitations with $\Delta t < 0.5\,\mathrm{s}$ are predicted with a high accuracy of 66-71%. Also, predictions of long visitations with $\Delta t > 1.5\,\mathrm{s}$ are relatively accurate. However, again all the prediction in-between show insufficient accuracies and are in majority too pessimistic. The performance of the different predictors is very similar. All the methods are unable to give good predictions, except for the extreme cases of very short or very long durations. The velocity predictors show the lowest accuracies in predicting entries and exits. The linear torque extrapolation shows overall the highest accuracy.

5.3 Error Margins

In the following section it is estimated, how accurate a prediction method would need to be to achieve satisfying results. The actual torque trajectory $\mathbf{T}_k^{Real}$ is perturbed by adding an error which increases linearly with rate f_{err}

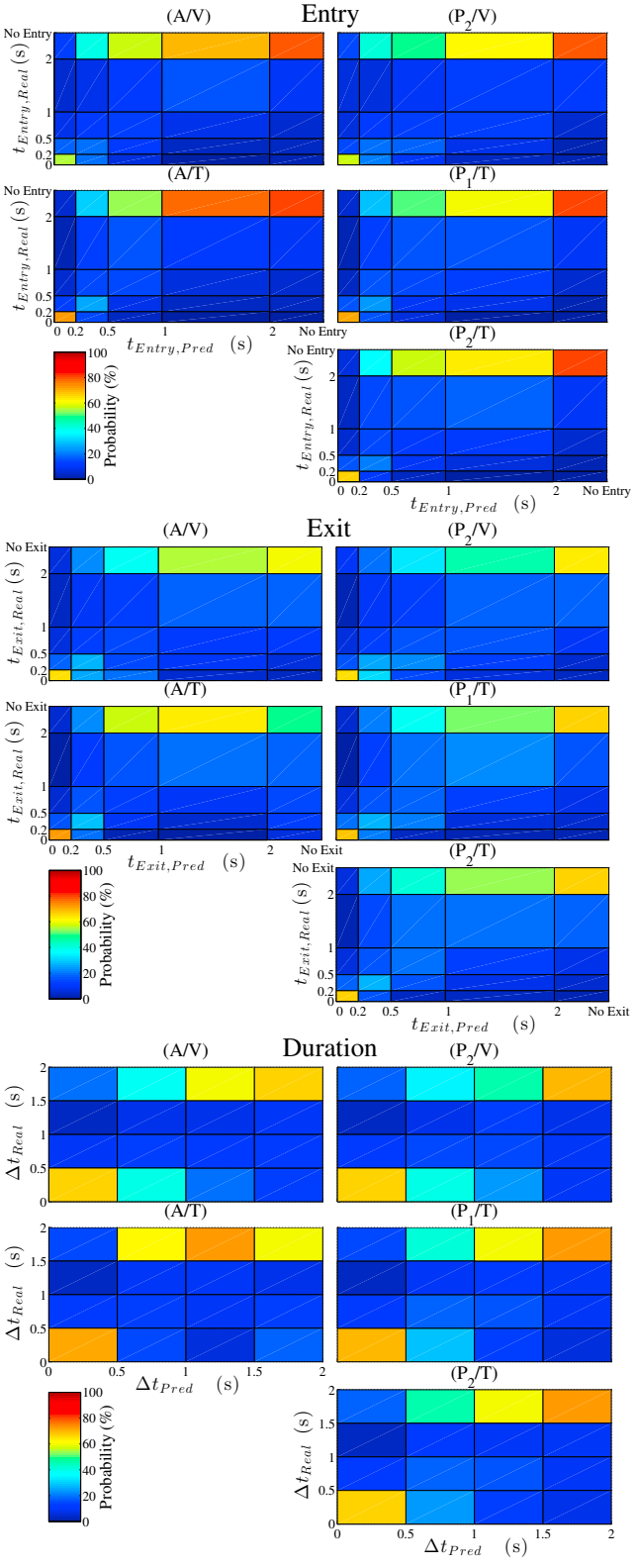

Fig. 12. Statistical correlation between the predicted and the actual HCCI entry (top third) and exit (center third) times as well as durations of visitations (bottom third) for the five prediction methods. The times are divided into bins. For a given prediction, the color represents the probability to end up with a certain actual time.

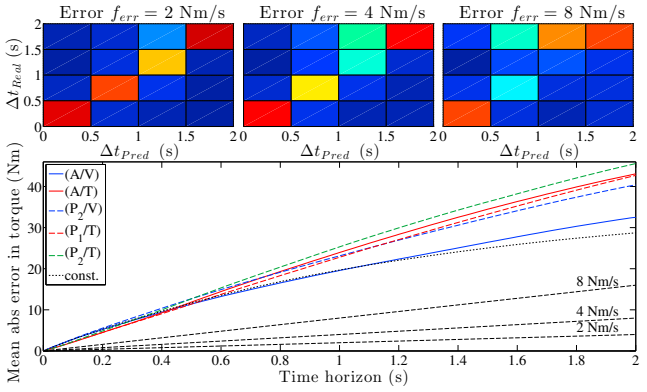

Fig. 13. Top: Statistical correlation between the predicted and the actual visitation duration of the HCCI regime for a prediction based on the actual behavior plus a linearly increasing error. Three different error slopes are compared. Bottom: Mean absolute error of the five predictors as a function of prediction time. In addition the three error slopes (dashed black).

$$T^k_{err,j} = \bar{T}_{k+j} \pm f_{err} \cdot j\tau_s \tag{32}$$

$$\mathbf{T}^{err}_k = \left(T^k_{err,k+1}, T^k_{err,k+2}, ..., T^k_{err,k+H}\right)^{\mathrm{T}}. \tag{33}$$

$\mathbf{T}^{err}_k$ is used as a prediction. This means, almost perfect knowledge of future torque with increasingly over or under prediction is assumed. The same analysis of duration of stay Δt was done for error rates $f_{err} = \{2\,\mathrm{Nm/s}, 4\,\mathrm{Nm/s}, 8\,\mathrm{Nm/s}\}$ and plotted on the top of Fig. 13. It can be seen that for a small error the distribution is still very close to diagonal. Even with $f_{err} = 4\,\mathrm{Nm/s}$ a prediction of stays up to 1 s can still be made. However, the case of $f_{err} = 8\,\mathrm{Nm/s}$ is already very similar to the ones in Fig. 12. On the bottom of Fig. 13 those three slopes are compared with the mean absolute error of the five prediction methods. As can be seen, all those methods show in average significantly larger error rates than $8\,\mathrm{Nm/s}$. Note that the two velocity predictors show a decreasing error rate compared to the torque predictors.

6. DISCUSSION

To make an optimal mode switch decision it would be preferable to have an accurate torque prediction over a short horizon. However, the results above suggest that this is difficult. It is surprising to see in Fig. 9 how a naive predictor assuming constant load performs in average better than all the prediction methods. However, it is impossible to predict HCCI entry and exit times by assuming the load to remain constant.

One large difficulty seems to originate from the strong nonlinearity in the driver's torque response. In addition modeling and measurement errors result in less accurate predictions. Therefore it was deemed important to test prediction methods against actual drive cycle measurement and not simulation data, which is generally smoother and more predictable. Maybe a different parameter offers better potential for prediction such as commanded torque by the ECU or the accelerator pedal position. Upcoming generations of vehicles will offer capabilities for V2X communication. Such technologies will provide valuable information to make predictions of future vehicle and engine

states. It must be tested if this data increases prediction accuracy and enables optimal SI/HCCI mode switching decisions.

Until then, based on the comparison of the different predictors above, it can be seen that none of the predictors is accurate enough to allow an optimal decision for visitation durations between $0.5\,\mathrm{s} < \Delta t < 1.5\,\mathrm{s}$. Therefore, visitations slightly too short to lead to fuel efficiency benefits cannot be predicted. Visitations with $\Delta t < 0.5\,\mathrm{s}$ can, however, be predicted with any of the presented methods. Therefore if constraints posed by mode switch fuel penalties, drivability, or hardware restrict the use of a simply reactive supervisory control strategy, some prediction could be used to improve performance.

It can be seen that the prediction shows high accuracy for immediate HCCI boundary crossings. This would allow for some time to prepare the mode switch, thereby alleviating potential issues concerning drivability. It is also able to predict very short visitations of the HCCI regime relatively well. For such a reduced strategy, a linear torque extrapolation seems to be the preferable choice, due to its simplicity. Based on the load extrapolation the predicted HCCI entry time $\hat{t}_{HCCI,Entry}$ and the predicted duration of a visitation of HCCI $\Delta\hat{t}_{HCCI}$ can be derived. If the entry time is closer than the time required to prepare the mode switch $\hat{t}_{HCCI,Entry} \leq d_{s,1}$ and the predicted duration of the visitation $\Delta\hat{t}_{HCCI} > 0.5s$, the mode switch should be prepared. As soon as HCCI is entered and still $\Delta\hat{t}_{HCCI} > 0.5s$, the cam switch should be conducted. On the other hand if $\Delta\hat{t}_{HCCI}$ increases above some threshold it can be assumed that the prediction was wrong, and it should be returned to standard SI. Vice versa for the HCCI/SI mode switch, if $\hat{t}_{HCCI,Exit}$ is smaller than the time requirement then the strategy should be to start preparing the switch.

7. CONCLUSION

Based on steady-state engine maps and combustion mode switch experiments the required residence time in HCCI combustion to lead to a fuel economy benefit was estimated to be around 1.2 s. Different receding horizon prediction methods were assessed with chassis dynamometer experiments. The methods based on ANN and polynomial fits were compared in terms of their general accuracy in load prediction as well as their forecast of HCCI entry and exit events. For the given engine data and all the methods compared, it was seen that the prediction accuracy for visitations of the HCCI regime with durations around 1.2 s is very low. Overall a linear extrapolation of engine torque showed the best performance. In future work, a supervisory control structure, based on determining an immediate HCCI entry or exit, will be implemented in simulation and tested in terms of fuel economy and drivability. Combustion mode switch measurement data will be used to extend the parameterization of the associated model to other operating conditions.

REFERENCES

Gorzelic, P., Shingne, P., Martz, J., Sterniak, J., Jiang, L., and Stefanopoulou, A. (2014). A low-order HCCI model extended to capture SI-HCCI mode transition data with two-stage cam switching. In *DSCC*.

Kulzer, A., Hathout, J.P., Sauer, C., Karrelmeyer, R., Fischer, W., and Christ, A. (2007). Multi-mode combustion strategies with CAI for a GDI engine. In *SAE*, 2007-01-0214.

Matsuda, T., Wada, H., Kono, T., Nakamura, T., and Urushihara, T. (2008). A study of a gasoline-fueled HCCI engine - mode changes from SI combustion to HCCI combustion. In *SAE*, 2008-01-0050.

Nüesch, S., Gorzelic, P., Jiang, L., Sterniak, J., and Stefanopoulou, A. (2015). Accounting for combustion mode switch dynamics and fuel penalties in drive cycle fuel economy. *International Journal of Engine Research*.

Nüesch, S., Hellström, E., Jiang, L., and Stefanopoulou, A. (2014). Mode switches among SI, SACI, and HCCI combustion and their influence on drive cycle fuel economy. In *ACC*, 849–854.

Sun, C., Hu, X., Sun, F., and Moura, S. (2014). Comparison of velocity forecasting strategies for predictive control in HEVs. In *DSCC*.

Thring, R. (1989). Homogeneous charge compression ignition (HCCI) engines. In *SAE Int. Fall Fuels and Lubricants Meeting and Exhibition*.

Zhang, S. and Zhu, G. (2014). Model-based mode transition control between SI and HCCI combustion. In *DSCC*.

Zhao, F., Asmus, T., Assanis, D., Dec, J., Eng, J., and Najt, P. (2003). Homogeneous charge compression ignition (HCCI) engine: Key research and development issues. *Warrendale, PA: Society of Automotive Engineers, 2003. 646*.